NANO LETTERS
Letter
Cite This: Nano Lett. 2019, 19, 2434−2442
pubs.acs.org/NanoLett

Quasi-Ballistic Thermal Transport Across MoS_2 Thin Films

Aditya Sood,[*,†,‡,◆] Feng Xiong,[§] Shunda Chen,[∥] Ramez Cheaito,[‡] Feifei Lian,[†,¶] Mehdi Asheghi,[‡] Yi Cui,[⊥,#] Davide Donadio,[∥,∇] Kenneth E. Goodson,[‡,⊥] and Eric Pop[*,†,⊥,○]

[†]Department of Electrical Engineering, Stanford University, Stanford, California 94305, United States
[‡]Department of Mechanical Engineering, Stanford University, Stanford, California 94305, United States
[§]Department of Electrical and Computer Engineering, University of Pittsburgh, Pittsburgh, Pennsylvania 15261, United States
[∥]Department of Chemistry, University of California, Davis, California 95616, United States
[⊥]Department of Materials Science and Engineering, Stanford University, Stanford, California 94305, United States
[#]Stanford Institute for Materials and Energy Sciences, SLAC National Accelerator Laboratory, Menlo Park, California 94025, United States
[∇]Ikerbasque, Basque Foundation for Science, E-48011 Bilbao, Spain
[○]Precourt Institute for Energy, Stanford University, Stanford, California 94305, United States

Supporting Information

ABSTRACT: Layered two-dimensional (2D) materials have highly anisotropic thermal properties between the in-plane and cross-plane directions. Conventionally, it is thought that cross-plane thermal conductivities (κ_z) are low, and therefore *c*-axis phonon mean free paths (MFPs) are small. Here, we measure κ_z across MoS_2 films of varying thickness (20−240 nm) and uncover evidence of very long *c*-axis phonon MFPs at room temperature in these layered semiconductors. Experimental data obtained using time-domain thermoreflectance (TDTR) are in good agreement with first-principles density functional theory (DFT). These calculations suggest that ~50% of the heat is carried by phonons with MFP > 200 nm, exceeding kinetic theory estimates by nearly 2 orders of magnitude. Because of quasi-ballistic effects, the κ_z of nanometer-thin films of MoS_2 scales with their thickness and the volumetric thermal resistance asymptotes to a nonzero value, ~10 m^2 K GW^{-1}. This contributes as much as 30% to the total thermal resistance of a 20 nm thick film, the rest being limited by thermal interface resistance with the SiO_2 substrate and top-side aluminum transducer. These findings are essential for understanding heat flow across nanometer-thin films of MoS_2 for optoelectronic and thermoelectric applications.

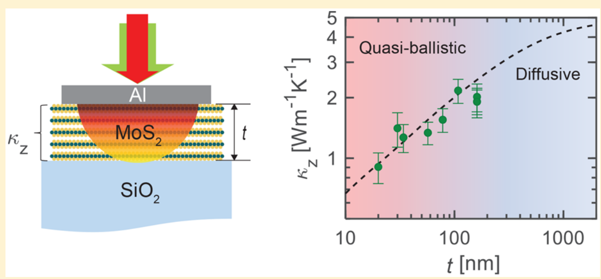

KEYWORDS: *Phonon, mean free path, MoS_2, cross-plane, thermal conductivity, time-domain thermoreflectance*

Two-dimensional (2D) van der Waals (vdW) layered solids have highly unusual thermal transport properties due to their unique crystal structure. While atoms within a layer are bonded covalently, adjacent layers are coupled via weak vdW interactions. This leads to a strong anisotropy in thermal conductivity, with the in-plane (along the layers) conductivity κ_r being significantly larger than the cross-plane (across the layers, or along the *c*-axis) conductivity κ_z. For example, in bulk graphite, h-BN, and MoS_2, anisotropy ratios (κ_r/κ_z) as high as ~300, 200, and 50, respectively, have been reported at room temperature.[1−3] Owing to their high κ_r, in-plane thermal transport in vdW layered materials has received significant attention, motivated in part by potential applications in heat spreading.[4,5]

In contrast, fundamental aspects of cross-plane thermal transport remain relatively underexplored, despite its relevance to nanoelectronics and energy harvesting applications. For example, self-heating plays a key role in limiting the performance of field effect transistors (FETs) made of 2D materials.[6,7] While some studies have characterized heat flow at single vdW interfaces,[8−12] very little is known about the physics of "intrinsic" cross-plane thermal transport across multiple vdW layers in layered thin films. Achieving a better understanding of this is critical to realizing the potential of 2D electronics, as previous work on multilayer MoS_2 transistors has shown enhancements in device mobility with increasing channel thickness (up to approximately tens of nanometers).[13,14] In such devices, charge screening and large interlayer electrical resistance can lead to the localization of current within the top few layers,[13] such that the dissipated heat must flow across multiple vdW interfaces before entering the substrate. It is therefore essential to understand the thickness dependence and fundamental limits of cross-plane thermal

Received: December 27, 2018
Revised: February 23, 2019
Published: February 27, 2019

DOI: 10.1021/acs.nanolett.8b05174
Nano Lett. 2019, 19, 2434−2442

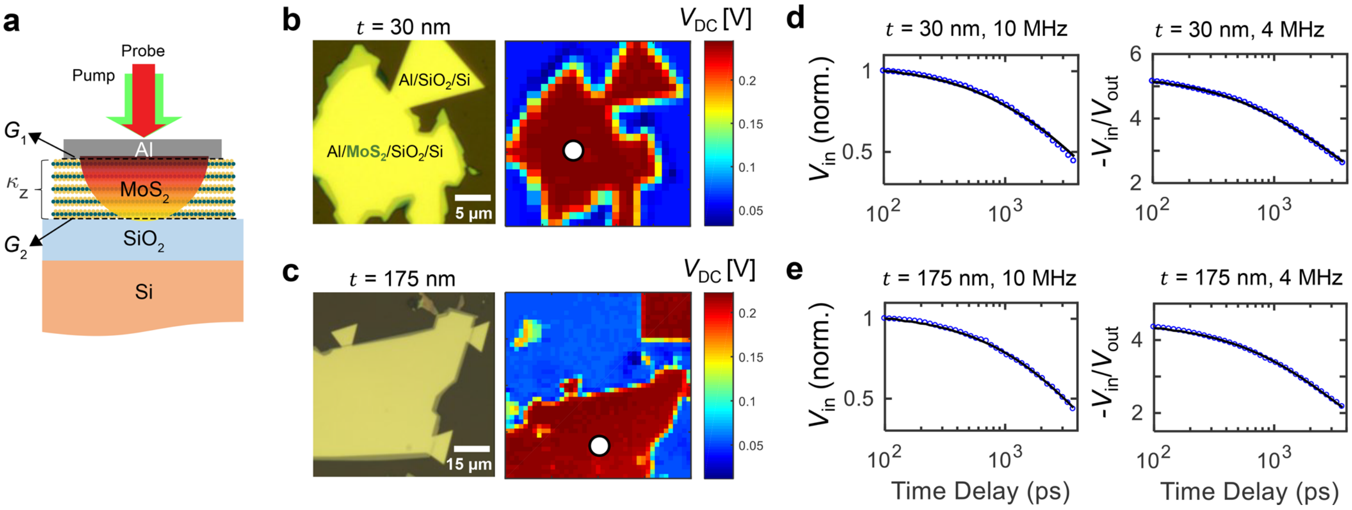

Figure 1. (a) Cross-sectional schematic of samples under study, showing the three unknown parameters: G_1 (TBC between Al and MoS_2), G_2 (TBC between MoS_2 and SiO_2), and κ_z (cross-plane thermal conductivity of MoS_2). The pump (green, 532 nm) and probe (red, 1064 nm) lasers used for TDTR are shown schematically. (b,c) Top view optical micrographs and probe reflectivity maps (taken at a fixed delay time of 0 ps) for 30 and 175 nm thick MoS_2 samples, respectively. Probe reflectivity maps are used to locate a uniform region away from the sample edges, where TDTR measurements are taken (white circles). (d,e) TDTR data (symbols) and best fits (lines): normalized in-phase signal V_{in} at f_{mod} = 10 MHz and $-V_{in}/V_{out}$ ratio at f_{mod} = 4 MHz for 30 and 175 nm thick films, respectively.

transport in vdW layered solids, particularly in materials like MoS_2.

A key quantity that determines thermal transport in the cross-plane direction of a material is the range of phonon mean free paths (MFPs) that carry heat. A simple estimate of the so-called gray MFP (Λ_z) can be made using the kinetic theory, $\kappa_z \sim (1/3)Cv_z\Lambda_z$; for MoS_2, using a heat capacity[15] $C \sim 2$ MJ m^{-3} K^{-1}, the average sound velocity of cross-plane acoustic modes[16] $v_z \sim 2400$ ms^{-1}, and the cross-plane bulk conductivity[3,17] $\kappa_z \sim 2-5$ W m^{-1} K^{-1}, gives a MFP of around 1.5−4 nm, which corresponds to a thickness of 2−6 layers. A similar calculation for graphite gives a gray MFP estimate of around 3 nm, corresponding to 9 layers. This would imply that size effects (i.e., thickness dependence of κ_z) should be negligible for films thicker than ∼10 nm, i.e. that the cross-plane thermal conductivity should be constant in this thickness regime. However, recent molecular dynamics (MD) simulations[18] and experimental measurements of κ_z in graphite[19,20] have suggested surprisingly long *c*-axis MFPs, on the order of approximately hundreds of nanometers.

These studies motivate the following key questions: (1) Are long *c*-axis phonon MFPs a general feature of other vdW-layered systems, like the transition metal dichalcogenides (TMDs) such as MoS_2? (2) Can experimental observations of long cross-plane phonon MFPs in vdW materials be explained by first-principles calculations? Density functional theory (DFT) has recently proven to be very effective in understanding fundamental aspects of thermal transport in covalently bonded systems like Si,[21] but similar studies are lacking for vdW-layered solids, especially quantitative comparisons with cross-plane thermal measurements. (3) What is the impact of cross-plane ballistic transport and related size effects on the thermal resistance of thin-film TMD devices? For monolayers, it is understood that interfaces dominate cross-plane transport.[8−11] However, the transition from interface-dominated to bulk-like transport across multilayer TMDs remains unclear to date.

In response, here we probe the spectrum of heat-carrying *c*-axis phonon MFPs in MoS_2, a vdW layered semiconductor. Through time-domain thermoreflectance (TDTR)[22] measurements of the thickness-dependent cross-plane thermal conductivity in single-crystalline films, we show that the *c*-axis phonon MFPs are at least ∼10s of nm long, significantly larger than kinetic theory estimates. Using first-principles DFT calculations we uncover that nearly 80% of the heat at room temperature is carried by phonons with MFPs in the range 10 to 500 nm. Furthermore, we show that by suitably defining a characteristic thermal length scale, our thickness-dependent κ_z data (with film thickness t ranging from 20 to 240 nm) are consistent with TDTR data on bulk MoS_2 crystals reported previously[3,17,23] (with thermal penetration depth d_p ranging from 200 nm to 1 μm). Taken together, we find good agreement between the combined data set and DFT predictions over a broad spectrum of thermal length scales, from 20 nm to 1 μm. Finally, using our measured values of the metal/MoS_2 and MoS_2/substrate interface resistances, we estimate the impact of cross-plane quasi-ballistic phonon transport on the total thermal resistance of multilayer MoS_2 devices. These calculations reveal that contrary to what is typically assumed, the total thermal resistance of few nanometer thick films is not entirely interface-dominated; the lower limit is set by the ballistic resistance across the thickness of MoS_2, which is estimated to be ∼10 m^2 K GW^{-1}.

Experimental Procedure. Single crystalline MoS_2 films were exfoliated onto SiO_2 (90 nm) on p-doped Si substrates using micromechanical exfoliation. Exfoliation yielded several MoS_2 films of different thicknesses on a single ∼1 cm^2 chip. Suitable films were identified using optical microscopy, and their thicknesses measured using atomic force microscopy (AFM). An ∼80 nm thick Al transducer was patterned and deposited onto the samples using electron-beam (e-beam) lithography and e-beam evaporation, respectively, for TDTR measurements (see sample schematic in Figure 1a and Methods). We also patterned Al onto bare regions of the SiO_2/Si substrate adjacent to the MoS_2 during the same

DOI: 10.1021/acs.nanolett.8b05174
Nano Lett. 2019, 19, 2434−2442

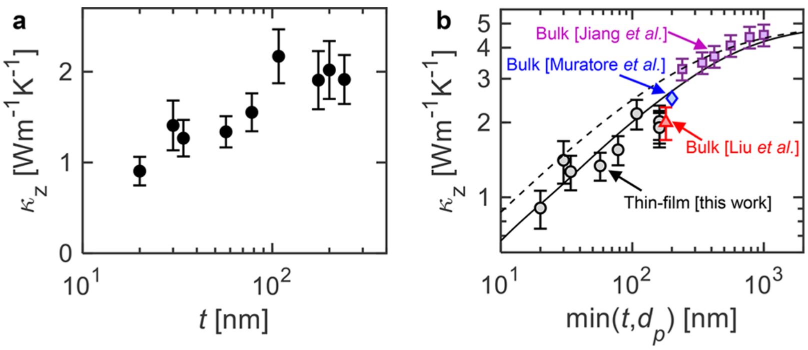

Figure 2. (a) Measured intrinsic cross-plane thermal conductivity κ_z versus film thickness t. (b) Experimental data plotted as a function of the characteristic thermal length scale, which is the smaller of the thickness (t) and thermal penetration depth (d_p). For our measurements, $d_p \approx 160$ nm in the three thickest films at $f_{mod} = 4$ MHz. Also shown are prior TDTR measurements of bulk MoS_2 by Liu et al.[3] (red triangle), Muratore et al.[23] (blue diamond), and Jiang et al.[17] (magenta squares). Solid and dashed lines are predictions of first-principles DFT calculations with suppression functions based on the BTE[20] (eq 2) and Matthiessen's rule (eq 3), respectively.

evaporation step. This allowed us to perform reference measurements of the SiO_2 next to each set of samples, and helped calibrate the accuracy and consistency of our setup.

Thermal transport measurements were made using TDTR, which is a well-established optical pump-probe technique capable of measuring thermal transport in thin films and across interfaces. Details of this technique and our setup have been described previously.[22] In these experiments, the pump beam was modulated at frequencies $f_{mod} = 4$ and 10 MHz. We used a high-magnification 50× objective lens that produced a focused root-mean-square (rms) spot size ($1/e^2$ diameter) of $w_0 \approx 3$ μm. An integrated dark-field microscope helped locate the samples under the laser spot.[24] Because some of the samples have lateral dimensions as small as 15 μm (especially for the thinnest films), it is important to position the laser spot well inside the edges of the flake. To do this, a precision two-axis translation stage was used to map out the TDTR signal and probe beam reflectivity over the area of the sample at a fixed delay time (see Figure 1b,c). A spot was chosen at the center of the sample within a region where the TDTR lock-in voltages and probe reflectivity were uniform, and TDTR scans were taken at that location with pump-probe delay times of 100 ps to 3.7 ns. The analysis scheme discussed below was used to simultaneously fit the normalized in-phase signal V_{in}, and the ratio ($= -V_{in}/V_{out}$) to a three-dimensional (3D) heat diffusion model that considers anisotropic transport.[1]

The sample stack consists of $Al/MoS_2/SiO_2/Si$ (see Figure 1a). The thicknesses of Al and MoS_2 were measured using AFM, while the SiO_2 thickness was characterized using ellipsometry to be 90 ± 1 nm. All measurements were performed at room temperature. The thermal conductivity of Al was estimated using in-plane electrical conductivity measurements on a patterned 4-probe device and the Wiedemann–Franz law, $\kappa_{Al} \approx 170$ W m^{-1} K^{-1}. The thermal conductivity of the p-type Si substrate, and volumetric specific heat of Al, SiO_2, MoS_2 and Si were taken from literature.[15,25–28] To reduce the uncertainties associated with slight variations in the laser spot size between measurements on different samples, reference data were taken on the $Al/SiO_2/Si$ regions next to each flake. Adjustments were made in the spot size (<5% variation across samples) to keep the fitted SiO_2 thermal conductivity fixed at 1.4 W m^{-1} K^{-1}. No f_{mod} dependence was observed in the thermal conductivity of SiO_2 and thermal boundary conductance (TBC) of the Al/SiO_2 interface (≈ 130 MW m^{-2} K^{-1}) for modulation frequencies between 4 and 10 MHz.

In the MoS_2 sample stack, there are four unknown parameters for each sample thickness t. They are the intrinsic cross-plane and in-plane thermal conductivities of the MoS_2 layer, κ_z and κ_r, and the TBCs at the Al/MoS_2 and MoS_2/SiO_2 interfaces, G_1 and G_2, respectively. The in-plane thermal conductivity is held fixed at $\kappa_r = 90$ W m^{-1} K^{-1}, based on prior measurements of bulk MoS_2 crystals by Liu et al.[3] Here, the authors had measured a spot-size dependent κ_r, likely due to the partial exclusion of ballistic phonons with in-plane MFPs larger than the spot diameter. Our estimate for κ_r is obtained by linearly interpolating their data to an rms spot diameter of 3 μm. To simplify our analysis we assume that κ_r is independent of t, at least within the range of thicknesses (20 nm < t < 240 nm) measured here. This is consistent with previous arguments by Minnich[29] and Gu et al.,[30] an assump-assumption further discussed below.

This assumption leaves three unknown parameters for each sample: κ_z, G_1, and G_2. To extract a unique value for κ_z, we use a combination of V_{in} and ratio ($= -V_{in}/V_{out}$) signals, at two different modulation frequencies, 4 and 10 MHz. This tandem fitting approach is similar to that used by Meyer et al.[31] and is supported by our sensitivity analysis (see Supporting Information Section 1). For films with t < 150 nm, we first estimate G_1 by fixing κ_z and G_2 and fitting the in-phase signal V_{in} (normalized at +100 ps) at the higher f_{mod} of 10 MHz. Next, fixing G_1 at this value, the voltage ratio data at the lower f_{mod} of 4 MHz are fit for κ_z and G_2. This process is repeated until the values of κ_z, G_1, and G_2 each change by less than 1% between successive iterations. We verify that the final fit results are not sensitive to the choice of initial values. For films with t > 150 nm, measurement sensitivity to the bottom interface TBC, G_2, is relatively low. For these, we follow the same procedure as above, except that G_2 is held fixed at 21 ± 5 MW m^{-2} K^{-1} based on the thin film results, further discussed below. Our methodology is generally similar to that used by Zhang et al.[20] and Jang et al.[32] for thickness-dependent κ_z measurements of graphite and black phosphorus, respectively. Error bars are calculated by propagating uncertainties in the assumed thermophysical parameters, mainly the Al thickness (±1 nm) and rms laser spot size (±2%), and for the thick films also G_2 (±5 MW m^{-2} K^{-1}).

We note that a recent experimental study[33] reported thickness-dependent in-plane thermal conductivity of MoS_2

DOI: 10.1021/acs.nanolett.8b05174
Nano Lett. 2019, 19, 2434–2442

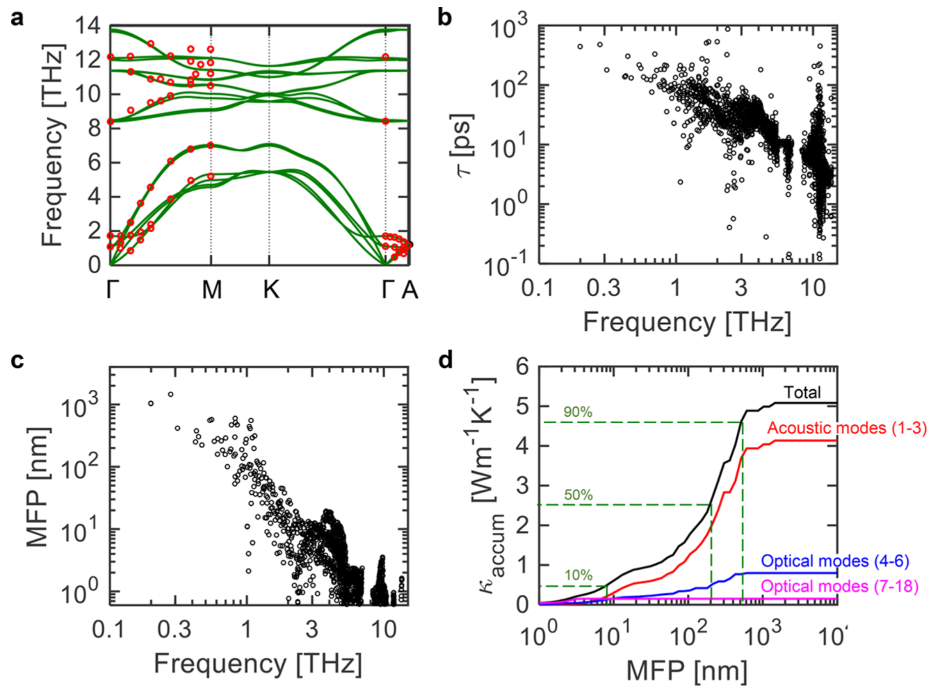

Figure 3. First-principles DFT calculations of MoS_2. (a) Phonon dispersion relations along high-symmetry directions in the Brillouin zone. Also shown with red circles are experimental data from neutron scattering on bulk MoS_2 crystals.[43] (b) Calculated phonon relaxation times, and (c) mean free paths (MFPs), plotted versus phonon frequency. (d) MFP accumulation function obtained from DFT calculations. The black curve is the total cross-plane thermal conductivity; the red, blue, and magenta curves are the contributions of the acoustic modes (branches 1−3, from low to high frequency on the dispersion relation), the three lowest-lying optical modes (branches 4−6), and the remaining higher-frequency optical modes (branches 7−18). Green dashed lines indicate MFPs corresponding to 10, 50, and 90% of the accumulated total thermal conductivity.

films in the range 2.4 to 37.8 nm. To check whether this thickness-dependence might affect our extraction of κ_z, we also analyzed our data using κ_r estimated from these results. For the 20 and 34 nm thick films, the resulting change in κ_z is only ∼2% and ∼12%, respectively. These uncertainties are within the experimental error bars; this further confirms that our assumption of constant κ_r for all films does not affect the extracted trend of κ_z versus t.

Results and Discussion. Representative TDTR data and model best fits for 30 and 175 nm thick samples are shown in Figure 1d,e, respectively. Figure S2 shows the extracted top and bottom interface TBCs, G_1 and G_2 versus t. The MoS_2/SiO_2 TBCs fall within a narrow range of 16 to 26 MW m^{-2} K^{-1}, in reasonable agreement with Raman thermometry measurements of monolayer MoS_2 on SiO_2 (14 ± 4 MW m^{-2} K^{-1}) by Yalon et al.[8,9] The Al/MoS_2 TBCs are in general higher than MoS_2/SiO_2 TBCs and also show a larger spread from 30 to 80 MW m^{-2} K^{-1} with no systematic trend as a function of t. This larger variability in G_1 could be a result of varying degrees of surface cleanliness after the e-beam patterning process that is used to define the Al transducer.

Figure 2a plots the extracted cross-plane thermal conductivity κ_z as a function of layer thickness t; κ_z for the thickest film (t = 240 nm) is 2.0 ± 0.3 W m^{-1} K^{-1}. This decreases with decreasing film thickness down to 0.9 ± 0.2 W m^{-1} K^{-1} for t = 20 nm, more than a two-fold reduction. Such a dependence of κ_z on t is indicative of quasi-ballistic c-axis phonon transport and suggests that the dominant heat-carrying vibrational modes have MFPs of at least tens of nanometers. We note that κ_z appears to saturate for the three thickest films. As discussed further below, we posit that this occurs due to the finite thermal penetration depth of the TDTR measurement.

Our measured κ_z values for the thickest films are close to two prior measurements of bulk MoS_2 by Liu et al.[3] and Muratore et al.[23] who obtained κ_z of ∼2 W m^{-1} K^{-1}, and ∼2.5 W m^{-1} K^{-1}, respectively, using a TDTR modulation frequency of 9.8 MHz.[34] However, these two results are significantly lower than recent measurements by Jiang et al.,[17] who obtained a bulk κ_z ∼4.8 W m^{-1} K^{-1}. In addition, our first-principles DFT calculations (described later) obtain a bulk κ_z ∼5 W m^{-1} K^{-1}, which is in good agreement with the experimental result of Jiang et al.[17] and a recent DFT calculation by Lindroth et al.[16] that predicted κ_z ∼5.1 W m^{-1} K^{-1}.

To understand possible reasons behind the apparent discrepancy among the different bulk κ_z measurements and first-principles calculations, we consider the characteristic thermal length scale (i.e., length scale over which the temperature gradient occurs) in the experiments. For TDTR measurements made at a frequency f_{mod}, this is determined by the thermal penetration depth[35] d_p, which is approximately $\sqrt{\kappa_z/\pi C f_{mod}}$. To calculate d_p accurately, we solve the full 3D heat diffusion equation in the two-layer Al/MoS_2 stack (see Supporting Information Section 3).

For the case of Liu et al.[3] and Muratore et al.,[23] this gives d_p ∼ 180 nm (for κ_z ∼2 W m^{-1} K^{-1}), and d_p ∼ 200 nm (for κ_z ∼2.5 W m^{-1} K^{-1}), respectively, at f_{mod} = 9.8 MHz. Jiang et al.[17] performed TDTR measurements of f_{mod}-dependent κ_z in bulk MoS_2, and observed a reduction in the apparent κ_z from 4.5 to 3.3 W m^{-1} K^{-1} while increasing f_{mod} from 1 to 10 MHz. These results were interpreted based on a two-channel model that considers nonequilibrium effects between low and high-frequency phonons that have different thermal conductivities and heat capacities. The interpretation of f_{mod}-dependent κ_z in modulated opto-thermal measurements has been the topic of

DOI: 10.1021/acs.nanolett.8b05174
Nano Lett. 2019, 19, 2434−2442

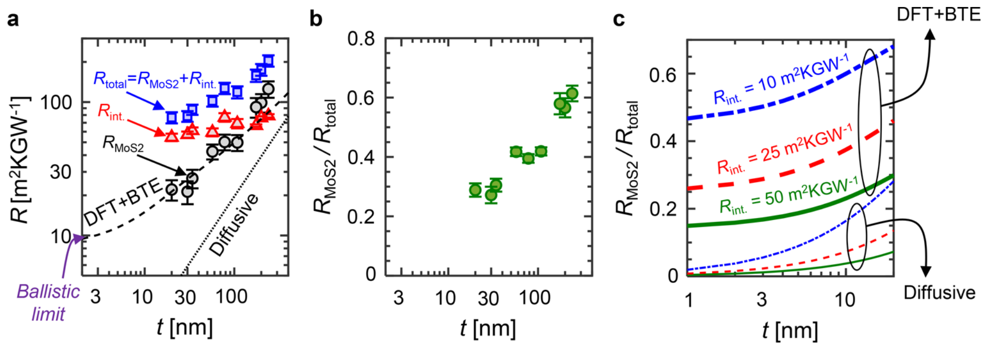

Figure 4. (a) Cross-plane thermal resistance of the MoS_2 film $R_{MoS2} = t/\kappa_z$ (black circles), combined thermal resistance of Al/MoS_2 and MoS_2/SiO_2 interfaces $R_{int.} = 1/G_1 + 1/G_2$ (red triangles), and total thermal resistance $R_{total} = R_{MoS2} + R_{int.}$ (blue squares), plotted versus film thickness t. The dashed line is the calculated quasi-ballistic R_{MoS2} based on first-principles MFPs (Figures 3c,d) and BTE suppression function (eq 2), while the dotted line is the corresponding diffusive calculation assuming a constant $\kappa_z = 5.1$ W m^{-1} K^{-1}. The y-intercept of the dashed line denotes the intrinsic cross-plane resistance in the ballistic limit ≈10 m^2 K GW^{-1}. (b) Fractional thermal resistance of the MoS_2 film compared to the total resistance (= R_{MoS2}/R_{total}) plotted versus t. (c) Calculated fractional resistance contributed by the MoS_2 film for sub-20 nm thicknesses. The quasi-ballistic (heavy lines) and diffusive case (light lines) are calculated in a manner similar to (a). Three cases are shown, corresponding to $R_{int.}$ = 10, 25, and 50 m^2 K GW^{-1} in the blue dash-dotted, red dashed, and green solid lines, respectively.

much recent discussion.[17,25,35−40] While the treatment of near-interfacial phonon nonequilibrium deserves further attention, a first order approximation is that the contributions to heat transport of long MFP phonons with $\Lambda_z > d_p$ are suppressed at high f_{mod}, thereby lowering the measured apparent κ_z. This simplification is reasonable for low thermal conductivity solids with relatively broad MFP spectra, as was discussed recently in the context of black phosphorus by Sun et al.,[41] and applied quantitatively to low thermal conductivity semiconductor alloys by Koh et al.[35]

In this simplified picture, we replot our thin-film κ_z data, along with the bulk data of Liu et al.,[3] Muratore et al.[23] and Jiang et al.,[17] against the thermal characteristic length scale (the smaller of t and d_p) as shown in Figure 2b. For our thin-film samples, d_p is calculated using a numerical solution of the 3D heat diffusion equation in the four-layer stack (Al/MoS_2/SiO_2/Si). For most of our films, d_p is larger than t. However, for the three thickest films $d_p \approx 160$ nm, which is smaller than t (= 175, 200, 240 nm). Details of these calculations are provided in the Supporting Information Section 3. Following this procedure, a combined data set is obtained, where κ_z increases from ~0.9 to ~5 W m^{-1} K^{-1} for thermal length scales ranging from 20 nm to 1 μm. This analysis suggests that one possible reason for the discrepancy between different bulk measurements[3,17,23] could be the dependence of κ_z on modulation frequency and the finite thermal penetration depth. However, given that the source of MoS_2 crystals is typically geological, one cannot entirely rule out differences in sample quality between the various studies as contributing to the observed κ_z variations.

Also shown in Figure 2b is a prediction of κ_z from first-principles calculations (described below), where the effect of finite thickness is incorporated with a suppression function calculated by the Boltzmann transport equation[20] (BTE) and Matthiessen's rule. These predictions show reasonably good agreement with the combined data set over the full range of characteristic thermal length scales from 20 nm to 1 μm. The data are thus consistent with theoretical predictions of very long c-axis phonon MFPs, and a broad spectral distribution of vibrational modes.

First-Principles DFT Calculations. To gain insight into fundamental aspects of phonon transport processes in MoS_2, we perform first-principles DFT calculations in the local density approximation of the exchange and correlation functional. We compute the frequency- and MFP-resolved κ_z of MoS_2 by solving the phonon BTE with an iterative self-consistent algorithm.[42] Further details are provided in Methods and Chen et al.[42]

Calculated phonon dispersion curves for 2H-MoS_2 are shown in Figure 3a, which are in good agreement with experimental data.[43] Figure 3b,c plots the calculated phonon relaxation times and MFPs as a function of phonon frequency. The MFP accumulation function κ_{accum} is calculated as a cumulative integral of the contributions to the total thermal conductivity of phonons with MFPs smaller than a certain value and is plotted in Figure 3d. From these calculations, we infer that more than 50% of the heat at room temperature is carried by phonons with MFPs exceeding 200 nm and nearly 80% is carried by MFPs in the range 10 to 500 nm. In comparison, in silicon,[21] 80% of the heat at room temperature is carried by phonons with MFPs between 40 nm and 10 μm.

On the basis of the MFP accumulation function, we calculate the cross-plane thermal conductivity of a film of thickness t as follows

$$\begin{aligned}\kappa_z(t) &= \int_0^\infty S(Kn_\omega)\kappa_{\text{partial}}(\Lambda_{z,\omega})d\Lambda_{z,\omega} \\ &= \int_0^\infty \frac{1}{t}N(Kn_\omega)\kappa_{\text{accum}}(\Lambda_{z,\omega})d\Lambda_{z,\omega}\end{aligned} \tag{1}$$

where $\kappa_{\text{partial}}(\Lambda_{z,\omega})$ is the MFP partial contribution function, $Kn_\omega = \Lambda_{z,\omega}/t$ is the Knudsen number, $S(Kn_\omega)$ is the heat flux suppression function, $\kappa_{\text{accum}}(\Lambda_{z,\omega}) = \int_0^{\Lambda_{z,\omega}} \kappa_{\text{partial}}(\Lambda_{z,\omega})d\Lambda_{z,\omega}$ is the MFP accumulation function, and $N(Kn_\omega) = -dS(Kn_\omega)/dKn_\omega$. Two cases are considered for the suppression function $S(Kn_\omega)$: one is based on a solution to the BTE for cross-plane heat flow in an anisotropic film inspired by the Fuchs−Sondheimer model[20] (eq 2), and the other is based on Matthiessen's rule (eq 3)

$$S_{\text{BTE}}(Kn_\omega) = 1 - Kn_\omega\left(1 - \exp\left(-\frac{1}{Kn_\omega}\right)\right) \tag{2}$$

DOI: 10.1021/acs.nanolett.8b05174
Nano Lett. 2019, 19, 2434−2442

$$S_{\mathrm{Matth.}}(Kn_{\omega}) = \frac{1}{1 + Kn_{\omega}} \tag{3}$$

These are plotted as solid and dashed lines, respectively, in Figure 2b and show good agreement with the experimental κ_z data over a large range of characteristic thermal length scales. These results have important implications for the design of thermoelectric devices based on vdW materials, as they suggest that cross-plane heat conduction can be suppressed significantly by the incorporation of defects along the *c*-axis,[42,44,45] such as intercalants and rotationally mismatched layers. The large phonon MFPs predicted and experimentally confirmed here offer a route to high-efficiency thermoelectrics based on nanostructuring of layered 2D materials along the *c*-axis.

Implications for 2D Device Thermal Characteristics. To understand the impact of cross-plane ballistic phonon transport on thermal characteristics of thin-film MoS_2 electronic and optoelectronic devices, in Figure 4a we plot the volumetric cross-plane thermal resistance $R_{MoS2} = t/\kappa_z$, the combined interface resistance (Al/MoS_2 and MoS_2/SiO_2) $R_{int.} = 1/G_1 + 1/G_2$, and the total thermal resistance $R_{total} = R_{MoS2} + R_{int.}$, as a function of thickness t. This simplification assumes that the total resistance can be decomposed into the separate interfacial and volumetric contributions even though a large fraction of phonons undergoes quasi-ballistic transport across the thickness of the MoS_2 film. This assumption, which is also inherent to our data analysis methodology, is consistent with the approach commonly followed in literature when dealing with subcontinuum heat conduction across thin films.[20]

We find that R_{MoS2} decreases with decreasing thickness but does not go to zero in the limit of zero t. This is a direct consequence of quasi-ballistic phonon transport and the diffusive scattering of long MFP phonons at the Al/MoS_2 and MoS_2/SiO_2 interfaces. In Figure 4a, we also plot the calculated MoS_2 volumetric resistance as a function of thickness, based on DFT predictions of the phonon MFPs and the BTE suppression function (eq 2). Because of ballistic transport across the film thickness, R_{MoS2} saturates at a finite value of ~10 m^2 K GW^{-1} in the limit of 2−3 monolayers. In the absence of quasi-ballistic effects, i.e., in the diffusive regime, R_{MoS2} would have been significantly lower and become vanishingly small in the monolayer limit.

An important consequence of quasi-ballistic effects is that the total thermal resistance is not dominated entirely by the interfaces, even for thin films. In Figure 4b we plot the fractional contribution of the volumetric MoS_2 resistance to the total device resistance ($= R_{MoS2}/R_{total}$) versus t. In our experiments, for the thinnest film (t = 20 nm), $R_{MoS2} \approx 22$ m^2 K GW^{-1} and $R_{total} \approx 76$ m^2 K GW^{-1}, i.e., nearly 30% of the total thermal resistance is due to the volumetric component. In the diffusive limit with constant $\kappa_z = 5.1$ W m^{-1} K^{-1}, this value is only 7% (i.e., the interfaces contribute 93%) for a 20 nm thick film. From a metrology perspective, an important consequence of this effect is our ability to experimentally measure the intrinsic component κ_z separately from the interface resistances, down to films as thin as 20 nm. If thermal transport were to remain diffusive, the volumetric resistance component would have been too small compared to the interface resistances, and we would not have been able to extract it uniquely using TDTR.

To estimate the contribution of quasi-ballistic transport to heat flow across thin devices ($t < 20$ nm), we plot the fractional MoS_2 volumetric component for different interface resistance values ($R_{int.}$= 10, 25, 50 m^2 K GW^{-1}), as shown in Figure 4c. As before, size effects are considered by calculating the thickness-dependent κ_z using the BTE suppression function described in eq 2 above. In the extreme scaling limit of 1−2 nm thick films (2−3 monolayers), we estimate this fractional contribution to be as large as ~15%, ~25%, and ~50% for $R_{int.}$= 50, 25, and 10 m^2 K GW^{-1}, respectively. This suggests that even if interface quality (and TBCs) of the $metal/MoS_2$ and MoS_2/substrate interfaces were to be improved substantially ($R_{int.} \to 0$), cross-plane heat transport would likely still be limited by the ballistic resistance ($= \lim_{t\to 0} t/\kappa_z$) of the MoS_2 film, which is ~10 m^2 K GW^{-1}. Note that this analysis assumes a 3D phonon dispersion for thin films, which may face its limits when the thickness becomes comparable to the phonon wavelengths (see Supporting Information Section 4). Nevertheless, this raises interesting questions about the nature of heat conduction across few-layer thick vdW layered materials, where it is often assumed that interfaces dominate the total cross-plane thermal resistance.[46] Given that the existence of long MFP *c*-axis thermal phonons has been experimentally demonstrated in graphite[19,20] and predicted theoretically in other TMDs such as WS_2 and WSe_2,[16] the above argument may be applicable to a large class of ultrathin vdW layered devices (see Supporting Information Section 5).

In conclusion, we reported thickness-dependent cross-plane thermal conductivity measurements of crystalline films of layered MoS_2. The cross-plane thermal conductivity shows a strong dependence on thickness in the range of 20−240 nm, revealing quantitative information about the distribution of phonon MFPs along the *c*-axis. Combining our results with previous measurements[3,17,23] of κ_z in bulk MoS_2 (made at different modulation frequencies) allowed us to map a large portion of the *c*-axis MFP spectrum from ~20 nm to ~1 μm. DFT calculations (with no fitting parameters) were able to obtain the thickness-dependent thermal conductivity over a large range of MFPs, illustrating the predictive power of first-principles phonon calculations for vdW layered materials.

Importantly, our results show for the first time that diffuse scattering of long MFP phonons imposes a lower limit on the cross-plane thermal resistance of vdW layered thin films. This can have significant implications for the thermal management of multilayer 2D electronics[13,47] and optoelectronics (e.g., photovoltaics) where thermal transport across the device thickness imposes the primary bottleneck for heat dissipation. Finally, the quantitative knowledge of thermal phonon MFPs obtained here will enable the design of new applications that require engineering of the phonon spectrum. For example, the substantial contribution of long MFP phonons to κ_z suggests that the introduction of disorder and defects along the *c*-axis can drastically suppress cross-plane thermal transport[45] without significantly affecting electronic transport. This could have exciting implications for cross-plane thermoelectrics made of layered 2D materials,[48] potentially enabling next-generation energy harvesting and electronics cooling technologies.

Methods. *Sample Preparation.* Flakes of MoS_2 were mechanically exfoliated from bulk crystals (SPI Supplies) onto 90 nm SiO_2 on p-type Si substrates (0.001 to 0.005 Ω.cm) using a thermal release tape (Nitto-Denko Revalpha). Samples were cleaned with an acetone/2-propanol soak and subsequently annealed in Ar/H_2 at 400 °C for 40 min. This was followed by spin coating a double layer of electron-beam (e-beam) resist PMMA 495 K A2/950 K A4 (Microchem).

DOI: 10.1021/acs.nanolett.8b05174
Nano Lett. 2019, 19, 2434−2442

The metal transducer (nominally 80 nm Al) was patterned by e-beam lithography (Raith 150, 10 kV) and deposited through e-beam evaporation. Lift-off was performed in acetone at 50 °C.

Ab Initio Calculations. First-principles phonon calculations of 2H-MoS_2 were carried out in the local density approximation (LDA) of the exchange and correlation functional using the Quantum-Espresso package.[49,50] Norm-conserving pseudopotentials were used to approximate core electrons.[51] Kohn−Sham wave functions were expanded on a plane wave basis set (cutoff = 100 Ry). Integration of the electronic properties over the first Brillouin zone was performed using 10 × 10 × 4 Monkhorst−Pack meshes of *k*-points.[52] Structural and cell relaxations were performed by a Broyden−Fletcher−Goldfarb−Shanno quasi-Newton algorithm with a strict convergence criterion of 10^{-8} Rydberg/Bohr for maximum residual force component.

Phonon dispersion relations were computed by density functional perturbation theory (DFPT)[53] with 10 × 10 × 4 *q*-point mesh (see Figure 3a). The computed dispersion curves agree well with neutron diffraction data for bulk MoS_2.[43] For the calculation of lattice thermal conductivity, anharmonic third order interatomic force constants (IFCs) are also necessary besides the harmonic second order IFCs. Third order anharmonic force constants were computed by finite differences for a supercell,[54] which is a 5 × 5 × 1 replica of the unit cell and contains 150 atoms, with an interaction cutoff of 7 Å, including interactions up to the tenth shell of neighbors. Translational invariance of the anharmonic force constants was enforced using the Lagrangian approach.[54] With the second and third order IFCs, the thermal conductivity of MoS_2 was computed by solving the phonon BTE with an iterative self-consistent algorithm, using the ShengBTE code,[54] considering phonon−phonon and isotopic scattering. Convergence was checked with *q*-point grids up to 45 × 45 × 11. Further details are provided in Chen et al.[42]

■ ASSOCIATED CONTENT

Supporting Information

The Supporting Information is available free of charge on the ACS Publications website at DOI: 10.1021/acs.nanolett.8b05174.

> TDTR sensitivity analysis. Thermal boundary conductance (TBC) measurements of Al/MoS_2 and MoS_2/SiO_2 interfaces. Calculations of thermal penetration depth. Phonon wavelength contributions to cross-plane thermal conductivity. Literature survey of cross-plane thermal resistance of few-layer graphene and thin-film graphite (PDF)

■ AUTHOR INFORMATION

Corresponding Authors

*E-mail: aditsood@alumni.stanford.edu.
*E-mail: epop@stanford.edu.

ORCID

Aditya Sood: 0000-0002-4319-666X
Shunda Chen: 0000-0002-5506-7507
Yi Cui: 0000-0002-6103-6352
Davide Donadio: 0000-0002-2150-4182
Eric Pop: 0000-0003-0436-8534

Present Addresses

◆(A.S.) Stanford Institute for Materials and Energy Sciences, SLAC National Accelerator Laboratory, Menlo Park, CA 94025, USA.
¶(F.L.) NG Next Basic Research Laboratory, Northrop Grumman Corporation, Redondo Beach, CA 90278, USA.

Author Contributions

A.S. and F.X. contributed equally. A.S., F.X., and E.P. conceived the project. A.S. designed and performed the TDTR measurements, analyzed experimental data, developed the theoretical model based on DFT calculations, and wrote the manuscript with input from E.P.; F.X. fabricated the samples; S.C. performed the DFT calculations; R.C. and F.L. provided inputs on data analysis; M.A., Y.C., D.D., K.E.G., and E.P. supervised the project.

Notes

The authors declare no competing financial interest.

■ ACKNOWLEDGMENTS

We acknowledge the Stanford Nanofabrication Facility (SNF) and Stanford Nano Shared Facilities (SNSF) for enabling device fabrication, funded under National Science Foundation (NSF) award ECCS-1542152. This work was supported in part by the NSF Engineering Research Center for Power Optimization of Electro Thermal Systems (POETS) with cooperative agreement EEC-1449548, by NSF EFRI 2-DARE Grant 1542883, by AFOSR Grant FA9550-14-1-0251, and by the Stanford SystemX Alliance. F.X. and Y.C. were partially supported by the Department of Energy, Office of Basic Energy Sciences, Division of Materials Science and Engineering, under contract DE-AC02-76SF00515.

■ REFERENCES

(1) Schmidt, A. J.; Chen, X.; Chen, G. Pulse Accumulation, Radial Heat Conduction, and Anisotropic Thermal Conductivity in Pump-Probe Transient Thermoreflectance. *Rev. Sci. Instrum.* **2008**, *79*, 114902.

(2) Sichel, E. K.; Miller, R. E.; Abrahams, M. S.; Buiocchi, C. J. Heat Capacity and Thermal Conductivity of Hexagonal Pyrolytic Boron Nitride. *Phys. Rev. B* **1976**, *13* (10), 4607−4611.

(3) Liu, J.; Choi, G. M.; Cahill, D. G. Measurement of the Anisotropic Thermal Conductivity of Molybdenum Disulfide by the Time-Resolved Magneto-Optic Kerr Effect. *J. Appl. Phys.* **2014**, *116*, 233107.

(4) Song, H.; Liu, J.; Liu, B.; Wu, J.; Cheng, H. M.; Kang, F. Two-Dimensional Materials for Thermal Management Applications. *Joule* **2018**, *2* (3), 442−463.

(5) Sood, A.; Pop, E.; Asheghi, M.; Goodson, K. E. The Heat Conduction Renaissance. 17th IEEE Intersociety Conference on Thermal and Thermomechanical Phenomena in Electronic Systems (ITherm); IEEE: 2018; pp 1396−1402.

(6) Suryavanshi, S. V.; Pop, E. S2DS: Physics-Based Compact Model for Circuit Simulation of Two-Dimensional Semiconductor Devices Including Non-Idealities. *J. Appl. Phys.* **2016**, *120*, 224503.

(7) Islam, S.; Li, Z.; Dorgan, V. E.; Bae, M. H.; Pop, E. Role of Joule Heating on Current Saturation and Transient Behavior of Graphene Transistors. *IEEE Electron Device Lett.* **2013**, *34* (2), 166−168.

(8) Yalon, E.; Mcclellan, C. J.; Smithe, K. K. H.; Xu, R. L.; Rojo, M. M.; Suryavanshi, S. V.; Gabourie, A. J.; Neumann, C. M.; Xiong, F.; Pop, E.; et al. Energy Dissipation in Monolayer MoS_2 Electronics. *Nano Lett.* **2017**, *17* (6), 3429−3433.

(9) Yalon, E.; Aslan, Ö. B.; Smithe, K. K. H.; McClellan, C. J.; Suryavanshi, S. V.; Xiong, F.; Sood, A.; Neumann, C. M.; Xu, X.; Goodson, K. E.; Heinz, T. F.; Pop, E. Temperature-Dependent Thermal Boundary Conductance of Monolayer MoS_2 by Raman

DOI: 10.1021/acs.nanolett.8b05174
Nano Lett. 2019, 19, 2434−2442

Thermometry. *ACS Appl. Mater. Interfaces* **2017**, *9* (49), 43013–43020.
(10) Yasaei, P.; Foss, C. J.; Karis, K.; Behranginia, A.; El-Ghandour, A. I.; Fathizadeh, A.; Olivares, J.; Majee, A. K.; Foster, C. D.; Khalili-Araghi, F.; Aksamija, Z.; Salehi-Khojin, A. Interfacial Thermal Transport in Monolayer MoS_2- and Graphene-Based Devices. *Adv. Mater. Interfaces* **2017**, *4*, 1700334.
(11) Liu, Y.; Ong, Z.; Wu, J.; Zhao, Y.; Watanabe, K.; Taniguchi, T.; Chi, D.; Zhang, G.; Thong, J. T. L.; Qiu, C.-W.; Hippalgaonkar, K. Thermal Conductance of the 2D MoS_2/h-BN and Graphene/h-BN Interfaces. *Sci. Rep.* **2017**, *7*, 43886.
(12) Yuan, P.; Li, C.; Xu, S.; Liu, J.; Wang, X. Interfacial Thermal Conductance between Few to Tens of Layered-MoS_2 and c-Si: Effect of MoS_2 Thickness. *Acta Mater.* **2017**, *122*, 152–165.
(13) Das, S.; Appenzeller, J. Screening and Interlayer Coupling in Multilayer MoS_2. *Phys. Status Solidi RRL* **2013**, *7* (4), 268–273.
(14) Cheng, R.; Jiang, S.; Chen, Y.; Liu, Y.; Weiss, N.; Cheng, H. C.; Wu, H.; Huang, Y.; Duan, X. Few-Layer Molybdenum Disulfide Transistors and Circuits for High-Speed Flexible Electronics. *Nat. Commun.* **2014**, *5*, 5143.
(15) Kim, J. Y.; Choi, S. M.; Seo, W. S.; Cho, W. S. Thermal and Electronic Properties of Exfoliated Metal Chalcogenides. *Bull. Korean Chem. Soc.* **2010**, *31* (11), 3225–3227.
(16) Lindroth, D. O.; Erhart, P. Thermal Transport in van Der Waals Solids from First-Principles Calculations. *Phys. Rev. B: Condens. Matter Mater. Phys.* **2016**, *94*, 115205.
(17) Jiang, P.; Qian, X.; Gu, X.; Yang, R. Probing Anisotropic Thermal Conductivity of Transition Metal Dichalcogenides MX_2 (M = Mo, W and X = S, Se) Using Time-Domain Thermoreflectance. *Adv. Mater.* **2017**, *29* (36), 1701068.
(18) Wei, Z.; Yang, J.; Chen, W.; Bi, K.; Li, D.; Chen, Y. Phonon Mean Free Path of Graphite along the *c*-Axis. *Appl. Phys. Lett.* **2014**, *104*, 081903.
(19) Fu, Q.; Yang, J.; Chen, Y.; Li, D.; Xu, D. Experimental Evidence of Very Long Intrinsic Phonon Mean Free Path along the *c*-Axis of Graphite. *Appl. Phys. Lett.* **2015**, *106*, 031905.
(20) Zhang, H.; Chen, X.; Jho, Y. D.; Minnich, A. J. Temperature-Dependent Mean Free Path Spectra of Thermal Phonons along the *c*-Axis of Graphite. *Nano Lett.* **2016**, *16* (3), 1643–1649.
(21) Esfarjani, K.; Chen, G.; Stokes, H. T. Heat Transport in Silicon from First-Principles Calculations. *Phys. Rev. B: Condens. Matter Mater. Phys.* **2011**, *84*, 085204.
(22) Sood, A.; Cho, J.; Hobart, K. D.; Feygelson, T. I.; Pate, B. B.; Asheghi, M.; Cahill, D. G.; Goodson, K. E. Anisotropic and Inhomogeneous Thermal Conduction in Suspended Thin-Film Polycrystalline Diamond. *J. Appl. Phys.* **2016**, *119*, 175103.
(23) Muratore, C.; Varshney, V.; Gengler, J. J.; Hu, J. J.; Bultman, J. E.; Smith, T. M.; Shamberger, P. J.; Qiu, B.; Ruan, X.; Roy, A. K.; Voevodin, A. A. Cross-Plane Thermal Properties of Transition Metal Dichalcogenides. *Appl. Phys. Lett.* **2013**, *102*, 081604.
(24) Sood, A.; Cheaito, R.; Bai, T.; Kwon, H.; Wang, Y.; Li, C.; Yates, L.; Bougher, T.; Graham, S.; Asheghi, M.; Goorsky, M.; Goodson, K. E. Direct Visualization of Thermal Conductivity Suppression Due to Enhanced Phonon Scattering near Individual Grain Boundaries. *Nano Lett.* **2018**, *18* (6), 3466–3472.
(25) Regner, K. T.; Sellan, D. P.; Su, Z.; Amon, C. H.; McGaughey, A. J. H.; Malen, J. A. Broadband Phonon Mean Free Path Contributions to Thermal Conductivity Measured Using Frequency Domain Thermoreflectance. *Nat. Commun.* **2013**, *4*, 1640.
(26) Shanks, H. R.; Maycock, P. D.; Sidles, P. H.; Danielson, G. C. Thermal Conductivity of Silicon from 300 to 1400 K. *Phys. Rev.* **1963**, *130* (5), 1743–1748.
(27) Buyco, E. H.; Davis, F. E. Specific Heat of Aluminum from Zero to Its Melting Temperature and Beyond. Equation for Representation of the Specific Heat of Solids. *J. Chem. Eng. Data* **1970**, *15* (4), 518–523.
(28) Flubacher, P.; Leadbetter, A. J.; Morrison, J. A. The Heat Capacity of Pure Silicon and Germanium and Properties of Their Vibrational Frequency Spectra. *Philos. Mag.* **1959**, *4* (39), 273–294.
(29) Minnich, A. J. Thermal Phonon Boundary Scattering in Anisotropic Thin Films. *Appl. Phys. Lett.* **2015**, *107*, 183106.
(30) Gu, X.; Li, B.; Yang, R. Layer Thickness-Dependent Phonon Properties and Thermal Conductivity of MoS_2. *J. Appl. Phys.* **2016**, *119*, 085106.
(31) Meyer, K. E.; Cheaito, R.; Paisley, E.; Shelton, C. T.; Braun, J. L.; Maria, J.; Ihlefeld, J. F.; Hopkins, P. E. Crystalline Coherence Length Effects on the Thermal Conductivity of MgO Thin Films. *J. Mater. Sci.* **2016**, *51* (23), 10408–10417.
(32) Jang, H.; Wood, J. D.; Ryder, C. R.; Hersam, M. C.; Cahill, D. G. Anisotropic Thermal Conductivity of Exfoliated Black Phosphorus. *Adv. Mater.* **2015**, *27* (48), 8017–8022.
(33) Yuan, P.; Wang, R.; Wang, T.; Wang, X.; Xie, Y. Nonmonotonic Thickness-Dependence of In-Plane Thermal Conductivity of Few-Layered MoS_2: 2.4 to 37.8 nm. *Phys. Chem. Chem. Phys.* **2018**, *20* (40), 25752–25761.
(34) Muratore, C. University of Dayton, Dayton, OH. Personal Communication, 2017.
(35) Koh, Y. K.; Cahill, D. G. Frequency Dependence of the Thermal Conductivity of Semiconductor Alloys. *Phys. Rev. B: Condens. Matter Mater. Phys.* **2007**, *76*, 075207.
(36) Wilson, R. B.; Feser, J. P.; Hohensee, G. T.; Cahill, D. G. Two-Channel Model for Nonequilibrium Thermal Transport in Pump-Probe Experiments. *Phys. Rev. B: Condens. Matter Mater. Phys.* **2013**, *88*, 144305.
(37) Wilson, R. B.; Cahill, D. G. Anisotropic Failure of Fourier Theory in Time-Domain Thermoreflectance Experiments. *Nat. Commun.* **2014**, *5*, 5075.
(38) Koh, Y. K.; Cahill, D. G.; Sun, B. Nonlocal Theory for Heat Transport at High Frequencies. *Phys. Rev. B: Condens. Matter Mater. Phys.* **2014**, *90*, 205412.
(39) Regner, K. T.; Wei, L. C.; Malen, J. A. Interpretation of Thermoreflectance Measurements with a Two-Temperature Model Including Non-Surface Heat Deposition. *J. Appl. Phys.* **2015**, *118*, 235101.
(40) Yang, F.; Dames, C. Heating-Frequency-Dependent Thermal Conductivity: An Analytical Solution from Diffusive to Ballistic Regime and its Relevance to Phonon Scattering Measurements. *Phys. Rev. B: Condens. Matter Mater. Phys.* **2015**, *91*, 165311.
(41) Sun, B.; Gu, X.; Zeng, Q.; Huang, X.; Yan, Y.; Liu, Z.; Yang, R.; Koh, Y. K. Temperature Dependence of Anisotropic Thermal-Conductivity Tensor of Bulk Black Phosphorus. *Adv. Mater.* **2017**, *29*, 1603297.
(42) Chen, S.; Sood, A.; Pop, E.; Goodson, K. E.; Donadio, D. Strongly Tunable Anisotropic Thermal Transport in MoS_2 by Strain and Lithium Intercalation: First Principles Calculations. *2D Mater.* **2019**. In press. DOI: 10.1088/2053-1583/ab0715.
(43) Wakabayashi, N.; Smith, H. G.; Nicklow, R. M. Lattice Dynamics of Hexagonal MoS_2 Studied by Neutron Scattering. *Phys. Rev. B* **1975**, *12* (2), 659–663.
(44) Zhu, G.; Liu, J.; Zheng, Q.; Zhang, R.; Li, D.; Banerjee, D.; Cahill, D. G. Tuning Thermal Conductivity in Molybdenum Disulfide by Electrochemical Intercalation. *Nat. Commun.* **2016**, *7*, 13211.
(45) Sood, A.; Xiong, F.; Chen, S.; Wang, H.; Selli, D.; Zhang, J.; McClellan, C. J.; Sun, J.; Donadio, D.; Cui, Y.; Pop, E.; Goodson, K. E. An Electrochemical Thermal Transistor. *Nat. Commun.* **2018**, *9*, 4510.
(46) Koh, Y. K.; Bae, M. H.; Cahill, D. G.; Pop, E. Heat Conduction across Monolayer and Few-Layer Graphenes. *Nano Lett.* **2010**, *10* (11), 4363–4368.
(47) Mleczko, M. J.; Xu, R. L.; Okabe, K.; Kuo, H.-H.; Fisher, I. R.; Wong, H.-S. P.; Nishi, Y.; Pop, E. High Current Density and Low Thermal Conductivity of Atomically Thin Semimetallic WTe_2. *ACS Nano* **2016**, *10* (8), 7507–7514.
(48) Kong, S.; Wu, T.; Yuan, M.; Huang, Z.; Meng, Q.-L.; Jiang, Q.; Zhuang, W.; Jiang, P.; Bao, X. Dramatically Enhanced Thermoelectric Performance of MoS_2 by Introducing MoO_2 Nanoinclusions. *J. Mater. Chem. A* **2017**, *5*, 2004–2011.

DOI: 10.1021/acs.nanolett.8b05174
Nano Lett. 2019, 19, 2434–2442

(49) Giannozzi, P.; Baroni, S.; Bonini, N.; Calandra, M.; Car, R.; Cavazzoni, C.; Ceresoli, D.; Chiarotti, G. L.; Cococcioni, M.; Dabo, I.; Dal Corso, A.; de Gironcoli, S.; Fabris, S.; Fratesi, G.; Gebauer, R.; Gerstmann, U.; Gougoussis, C.; Kokalj, A.; Lazzeri, M.; Martin-Samos, L.; Marzari, N.; Mauri, F.; Mazzarello, R.; Paolini, S.; Pasquarello, A.; Paulatto, L.; Sbraccia, C.; Scandolo, S.; Sclauzero, G.; Seitsonen, A. P.; Smogunov, A.; Umari, P.; Wentzcovitch, R. M. QUANTUM ESPRESSO: A Modular and Open-Source Software Project for Quantum Simulations of Materials. *J. Phys.: Condens. Matter* **2009**, *21* (39), 395502.

(50) Perdew, J. P.; Zunger, A. Self-Interaction Correction to Density-Functional Approximations for Many-Electron Systems. *Phys. Rev. B: Condens. Matter Mater. Phys.* **1981**, *23* (10), 5048−5079.

(51) Hartwigsen, C.; Goedecker, S.; Hutter, J. Relativistic Separable Dual-Space Gaussian Pseudopotentials from H to Rn. *Phys. Rev. B: Condens. Matter Mater. Phys.* **1998**, *58* (7), 3641−3662.

(52) Monkhorst, H. J.; Pack, J. D. Special Points for Brillouin-Zone Integrations. *Phys. Rev. B* **1976**, *13* (12), 5188−5192.

(53) Baroni, S.; De Gironcoli, S.; Dal Corso, A.; Giannozzi, P. Phonons and Related Crystal Properties from Density-Functional Perturbation Theory. *Rev. Mod. Phys.* **2001**, *73* (2), 515−562.

(54) Li, W.; Carrete, J.; Katcho, N. A.; Mingo, N. ShengBTE: A Solver of the Boltzmann Transport Equation for Phonons. *Comput. Phys. Commun.* **2014**, *185* (6), 1747−1758.

DOI: 10.1021/acs.nanolett.8b05174
Nano Lett. 2019, 19, 2434−2442

Supporting Information:

Quasi-Ballistic Thermal Transport Across MoS_2 Thin Films

Aditya Sood[1,2,†,‡,*], *Feng Xiong*[3,‡], *Shunda Chen*[4], *Ramez Cheaito*[2], *Feifei Lian*[1,¶], *Mehdi Asheghi*[2], *Yi Cui*[5,6], *Davide Donadio*[4,7], *Kenneth E. Goodson*[2,5], *Eric Pop*[1,5,8,*]

[1]Department of Electrical Engineering, Stanford University, Stanford, CA 94305, USA. [2]Department of Mechanical Engineering, Stanford University, Stanford, CA 94305, USA. [3]Department of Electrical and Computer Engineering, University of Pittsburgh, Pittsburgh, PA 15261, USA. [4]Department of Chemistry, University of California, Davis, CA 95616, USA. [5]Department of Materials Science and Engineering, Stanford University, Stanford, CA 94305, USA. [6]Stanford Institute for Materials and Energy Sciences, SLAC National Accelerator Laboratory, Menlo Park, CA 94025, USA. [7]Ikerbasque, Basque Foundation for Science, E-48011 Bilbao, Spain. [8]Precourt Institute for Energy, Stanford University, Stanford, CA 94305, USA. [†]Present address: Stanford Institute for Materials and Energy Sciences, SLAC National Accelerator Laboratory, Menlo Park, CA 94025, USA. [¶]Present address: NG Next Basic Research Laboratory, Northrop Grumman Corporation, Redondo Beach, CA 90278, USA. [‡]Equal contribution.

[*]Corresponding authors: aditsood@alumni.stanford.edu, epop@stanford.edu

1. TDTR sensitivity analysis

To determine TDTR measurement sensitivity to the different parameters of interest, we calculate the sensitivity coefficients S_α as follows:

$$S_\alpha = \frac{\partial \log(Signal)}{\partial \log(\alpha)}$$

where *signal* could either refer to the normalized *in-phase voltage* (V_{in}) or the *ratio* (= - V_{in}/V_{out}), and the parameter α could be the cross-plane thermal conductivity κ_z, the Al/MoS_2 thermal boundary conductance (TBC) G_1, or the MoS_2/SiO_2 TBC G_2. These are plotted in Figure S1 for a 20 nm thick film (a, b), and a 200 nm thick film (c, d).

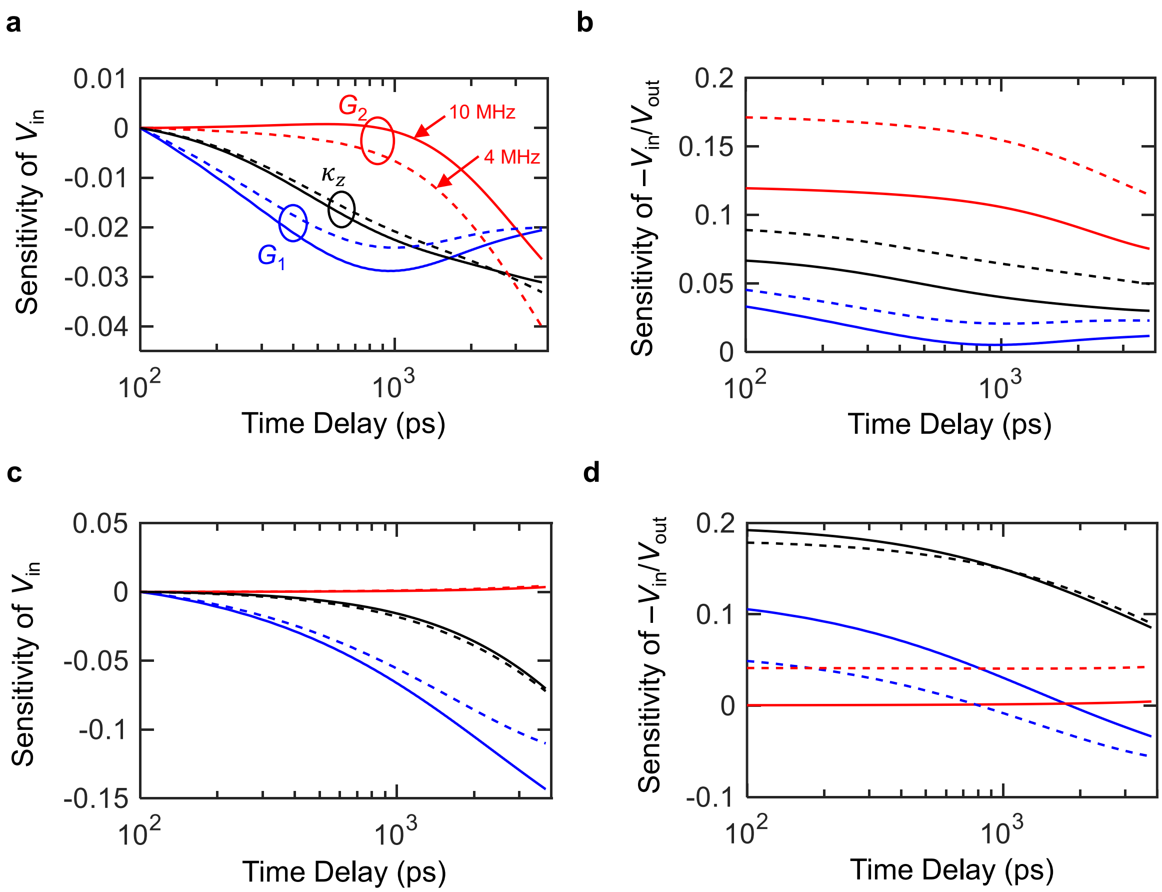

Figure S1. Sensitivity coefficients plotted for (a),(b): t = 20 nm, G_1 = 70 MWm^{-2}K^{-1}, G_2 = 25 MWm^{-2}K^{-1}, κ_z = 0.9 Wm^{-1}K^{-1}, and (c),(d): t = 200 nm, G_1 = 34 MWm^{-2}K^{-1}, G_2 = 21 MWm^{-2}K^{-1}, κ_z = 2 Wm^{-1}K^{-1}. Legend: black (κ_z), blue (G_1), red (G_2). Solid lines (10 MHz), dashed lines (4 MHz).

2. Thermal boundary conductance (TBC) measurements

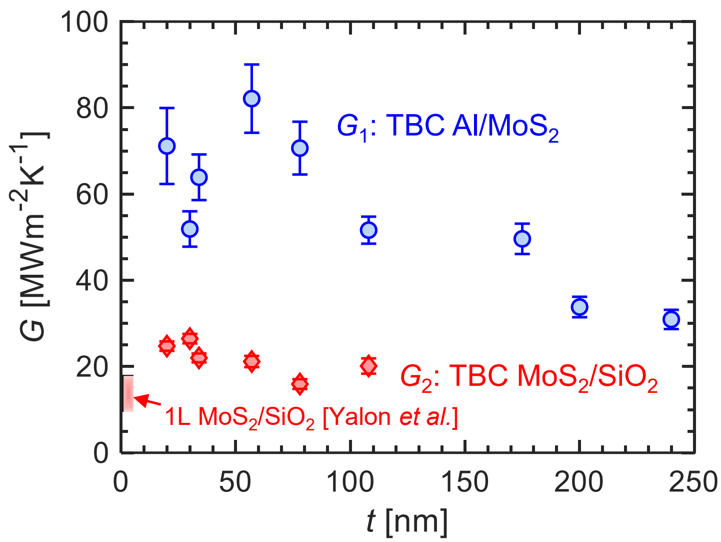

Figure S2. Al/MoS_2 (G_1) and MoS_2/SiO_2 (G_2) TBCs plotted versus film thickness t, shown by the blue circles and red diamonds, respectively. Also shown for comparison are TBC measurements between monolayer MoS_2 and SiO_2 obtained by Raman thermometry[1,2] (red shaded region represents the error bars of the reported result).

3. Thermal penetration depth calculations

To calculate the thermal penetration depth (d_p) in the TDTR measurements, we solve the full 3D heat diffusion equation in the multilayer stack. This is solved in the frequency domain under a sinusoidal heat flux excitation using methods described elsewhere[3,4]. We compute the amplitude of temperature oscillations $\Delta T(r, z)$ at the modulation frequency f_mod; d_p is the distance from the top surface at which $\Delta T(r, z)$ is reduced to $1/e$ of its maximum value.

Figure S3(a) shows $\Delta T(r, z)$ within a 300 nm thick MoS_2 film – this case is representative of one of the thick samples measured in our study (for which $\kappa_\mathrm{z} \sim 2$ $Wm^{-1}K^{-1}$). The simulation is carried out on a multilayer stack of Al/MoS_2/SiO_2/Si using a 4-layer model. The thermal properties of the various layers are provided in the main text. The TBCs of the Al/MoS_2 and MoS_2/SiO_2 interfaces are 40 $MWm^{-2}K^{-1}$ and 20 $MWm^{-2}K^{-1}$ respectively, although these do not affect d_p significantly. The heat flux is modulated at f_mod = 4 MHz, since this is the frequency at which we extract κ_z. Note that d_p is affected both by f_mod and the laser spot diameter (w_0); in these simulations, w_0 = 3 µm. Figure S3(b) plots $\Delta T(z)$ at r = 0. From this we estimate $d_\mathrm{p} \approx$ 160 nm.

The same procedure is used to calculate d_p for the bulk samples measured in previous studies[5–7] using a 2-layer model (Al/MoS_2). In each case, the simulations are performed using the reported κ_z, f_mod and w_0 values. A representative calculation[5] is shown in Figures S3(c),(d).

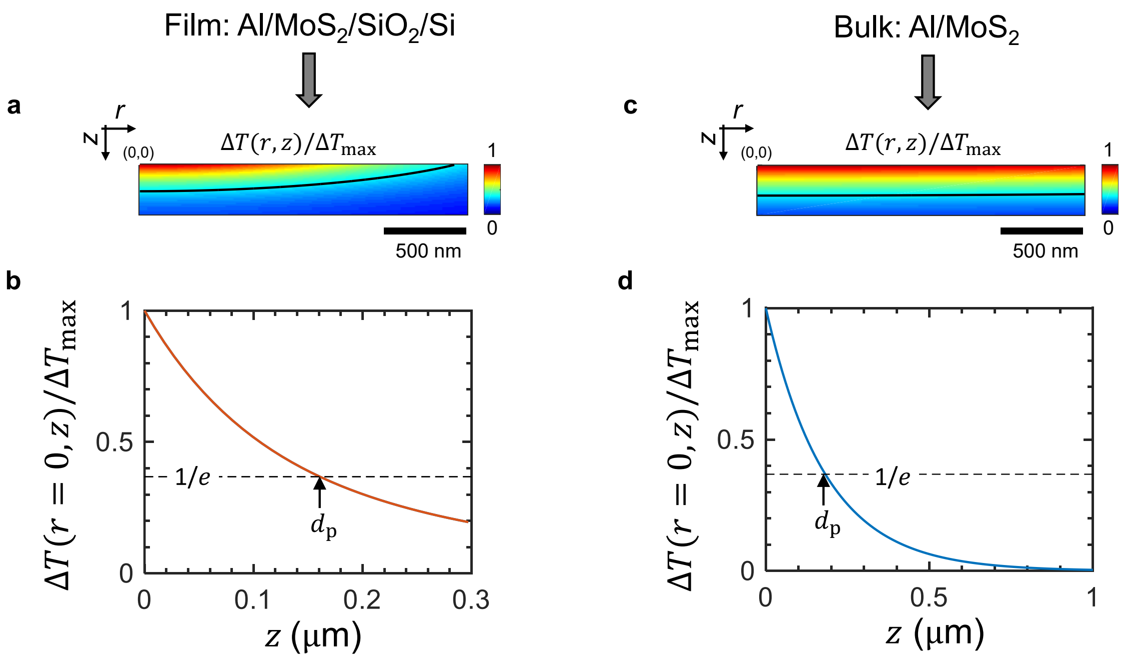

Figure S3. (a) Normalized amplitude of temperature oscillations in a 300 nm thick MoS_2 film with $\kappa_z = 2$ Wm^{-1}K^{-1}, $f_{\mathrm{mod}} = 4$ MHz, $w_0 = 3$ μm. The film is part of a multilayer stack: Al/MoS_2/SiO_2/Si, representative of the samples measured in this study. (b) Line-out along $r = 0$, with the dashed line indicating a $1/e$ thermal penetration depth of $d_{\mathrm{p}} \approx 160$ nm. (c) Normalized amplitude of temperature oscillations in a bulk MoS_2 substrate[5] with $\kappa_z = 2$ Wm^{-1}K^{-1}, $f_{\mathrm{mod}} = 9.8$ MHz, $w_0 = 24$ μm. (d) Line-out along $r = 0$, indicating $d_{\mathrm{p}} \approx 180$ nm.

4. Phonon wavelength contributions to thermal conductivity

We use DFT calculations to determine the range of phonon wavelengths that contribute to thermal transport along the c-axis. Figure S4 shows the thermal conductivity accumulation function plotted versus wavelength at 300 K. Based on this, the median wavelength is $\lambda \sim 1.5$ nm. If we posit that the MoS_2 film must have a thickness of at least $\sim 3\lambda$ in order to have a '3D' phonon dispersion, we estimate a minimum thickness of ~5 nm. For $t < 5$ nm, more detailed calculations may be needed to understand the effect of confinement on phonon band structure and cross-plane thermal transport.

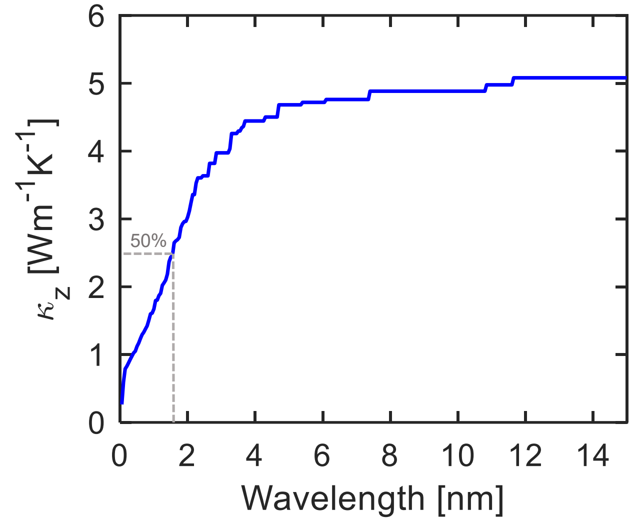

Figure S4. Calculated cumulative distribution function of the cross-plane thermal conductivity (κ_z) versus phonon wavelength at 300 K.

5. Cross-plane thermal transport in thin-film graphite and few-layer graphene

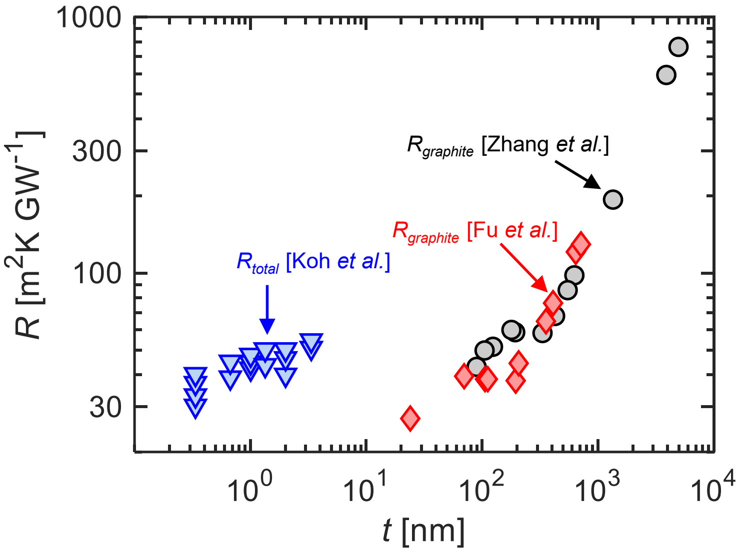

Figure S5. A summary of cross-plane thermal resistance measurements of crystalline graphite thin-films and few-layer graphene from literature. Intrinsic cross-plane thermal resistance measurements are from Zhang *et al.*[8] (90 nm < t < 5 µm), shown in black circles, and Fu *et al.*[9] (24 nm < t < 714 nm), shown in red diamonds. The intrinsic resistance is defined as $R_{\mathrm{graphite}} = t/\kappa_{\mathrm{z}}$. For the case of Fu *et al.*[9] this is calculated by subtracting out the estimated interface contribution. Total cross-plane thermal resistance measurements of Au/Ti/few-layer-graphene/SiO_2 interfaces for 0.3 < t < 3 nm are from Koh *et al.*[10], shown as blue triangles; the total resistance including the interfacial contribution is $R_{\mathrm{total}} = R_{\mathrm{n-graphene}} + R_{\mathrm{interfaces}}$. The plateau in intrinsic thermal resistance in Zhang *et al.*[8] and Fu *et al.*[9] could be related to the onset of quasi-ballistic thermal transport. A comparison to the total thermal resistance values for few-layer-graphene by Koh *et al.*[10] suggests that a contributing factor to the thickness-independent R_{total} could be the strongly-ballistic transport of thermal phonons propagating along the *c*-axis of the thin-films.

References

(1) Yalon, E.; Mcclellan, C. J.; Smithe, K. K. H.; Xu, R. L.; Rojo, M. M.; Suryavanshi, S. V.; Gabourie, A. J.; Neumann, C. M.; Xiong, F.; Pop, E. Energy Dissipation in Monolayer MoS_2 Electronics. *Nano Lett.* **2017**, *17* (6), 3429–3433.

(2) Yalon, E.; Aslan, Ö. B.; Smithe, K. K. H.; McClellan, C. J.; Suryavanshi, S. V.; Xiong, F.; Sood, A.; Neumann, C. M.; Xu, X.; Goodson, K. E.; Heinz, T. F.; Pop, E. Temperature-Dependent Thermal Boundary Conductance of Monolayer MoS_2 by Raman Thermometry. *ACS Appl. Mater. Interfaces* **2017**, *9* (49), 43013–43020.

(3) Cahill, D. G. Analysis of Heat Flow in Layered Structures for Time-Domain Thermoreflectance. *Rev. Sci. Instrum.* **2004**, *75* (12), 5119–5122.

(4) Braun, J. L.; Hopkins, P. E. Upper Limit to the Thermal Penetration Depth during Modulated Heating of Multilayer Thin Films with Pulsed and Continuous Wave Lasers: A Numerical Study. *J. Appl. Phys.* **2017**, *121*, 175107.

(5) Liu, J.; Choi, G. M.; Cahill, D. G. Measurement of the Anisotropic Thermal Conductivity of Molybdenum Disulfide by the Time-Resolved Magneto-Optic Kerr Effect. *J. Appl. Phys.* **2014**, *116*, 233107.

(6) Jiang, P.; Qian, X.; Gu, X.; Yang, R. Probing Anisotropic Thermal Conductivity of Transition Metal Dichalcogenides MX_2 (M = Mo, W and X = S, Se) Using Time-Domain Thermoreflectance. *Adv. Mater.* **2017**, *29* (36), 1701068.

(7) Muratore, C.; Varshney, V.; Gengler, J. J.; Hu, J. J.; Bultman, J. E.; Smith, T. M.; Shamberger, P. J.; Qiu, B.; Ruan, X.; Roy, A. K.; Voevodin, A. A. Cross-Plane Thermal Properties of Transition Metal Dichalcogenides. *Appl. Phys. Lett.* **2013**, *102*, 081604.

(8) Zhang, H.; Chen, X.; Jho, Y. D.; Minnich, A. J. Temperature-Dependent Mean Free Path

Spectra of Thermal Phonons along the *c*-Axis of Graphite. *Nano Lett.* **2016**, *16* (3), 1643–1649.

(9) Fu, Q.; Yang, J.; Chen, Y.; Li, D.; Xu, D. Experimental Evidence of Very Long Intrinsic Phonon Mean Free Path along the *c*-Axis of Graphite. *Appl. Phys. Lett.* **2015**, *106*, 031905.

(10) Koh, Y. K.; Bae, M. H.; Cahill, D. G.; Pop, E. Heat Conduction across Monolayer and Few-Layer Graphenes. *Nano Lett.* **2010**, *10* (11), 4363–4368.